The Astrophysical Journal, 983:123 (7pp), 2025 April 20 https://doi.org/10.3847/1538-4357/adc385

Revisiting Physical Properties of Mock Globular Cluster Tidal Tails

Andrés E. Piatti[1,2]
[1] Instituto Interdisciplinario de Ciencias Básicas (ICB), CONICET-UNCuyo, Padre J. Contreras 1300, M5502JMA, Mendoza, Argentina; andres.piatti@fcen.uncu.edu.ar
[2] Consejo Nacional de Investigaciones Científicas y Técnicas (CONICET), Godoy Cruz 2290, C1425FQB, Buenos Aires, Argentina
Received 2025 February 1; revised 2025 March 5; accepted 2025 March 18; published 2025 April 15

Abstract

In this work, we present results of the first in-depth analysis of extra-tidal mock stars of Milky Way globular clusters recently generated by S. M. Grondin et al. Particularly, we selected a sample of globular clusters with a general consensus of being formed in the bulge or in the disk of the Milky Way. From the catalog, we estimated the width and the dispersion in the z-component of the angular momentum and in the line-of-sight and tangential velocities of their tidal tails, and compared the results with those predicted by cosmological simulations of K. Malhan et al. and observations. We found that the resulting values of these four quantities are not in agreement with an in situ formation of the associated globular clusters. On average, the resulting widths agree with an in situ origin, while the dispersion in the z-component of the angular momentum, and the dispersion in the line-of-sight and tangential velocities fail in matching this formation scenario. The four quantities derived for globular clusters formed in the bulge or in the disk show similar correlations with the stream length, namely, the width and the dispersion in the z-component of the angular momentum increase with the stream length, while the bulk of dispersion values in the line-of-sight and tangential velocities is around 12 km s^{-1} along the mock stream.

Unified Astronomy Thesaurus concepts: Globular star clusters (656); Milky Way Galaxy (1054); Galaxy kinematics (602)

1. Introduction

It is known that globular clusters lose stars by tidal stripping during their lifetime, although only a percentage of them do already have detected tidal tails (S. Zhang et al. 2022). Some tidal tails have been targeted by detailed studies, which showed their complex physical structures (K. Malhan et al. 2019; A. Bonaca et al. 2020; T. J. L. de Boer et al. 2020; C. J. Grillmair 2022). Such tidal structures are the results of the dynamical evolution of globular clusters in the host galaxy gravitational field. Recently, S. M. Grondin et al. (2024) generated a catalog of mock extra-tidal stars for 159 Milky Way globular clusters, providing sky position, kinematics, and stellar properties for all simulated stars. These extra-tidal mock stars were generated from strong three-body encounters in the core of the globular clusters, which produce significantly higher ejection velocities (and dispersions) than the combination of weak two-body relaxation and tidal stripping that produce most stars in a tidal tail/stellar stream (e.g., L. Spitzer & S. L. Shapiro 1972; J. Binney & S. Tremaine 2008; N. C. Weatherford et al. 2023). Since S. M. Grondin et al. (2024) mock stars are not generated from accreted halos, their globular cluster formation reproduces the in situ scenario. They found that mock extra-tidal stars show very good agreement with tidal tail stars of the globular cluster Pal 13, used as a case study, so that the catalog has been made publicly available to help identify tidal tail stars whenever shallow observational data are available or they do not exist.

In order to assess at what extent these mock tidal tails represent those real ones, and therefore are suitable for further tidal tail investigations, we analyzed some of their physical properties to the light of the expected values for tidal tails primarily made up of lower-speed escapers ejected by two-body relaxation combined with tidal stripping as found by K. Malhan et al. (2021) and K. Malhan et al. (2022). These authors proposed that some morphological and dynamical properties of globular cluster tidal tails tell us about the origin of Milky Way globular clusters, namely, whether they were accreted or formed in situ. They showed that the width of tidal tails, and their dispersion in the z-component of the angular momentum, and in the line-of-sight and tangential velocities can help disentangle globular clusters' origin. Globular clusters formed in a low-mass galaxy halo with cored or cuspy central density profiles of dark matter that later merged with the Milky Way develop tidal tails with different mean values of the mentioned properties. On average, globular clusters from cuspy profiles have tidal tails with the above four properties being 3 times larger than those of clusters formed in cored dark matter profiles. Globular clusters formed in situ have mean values of these quantities nearly 10 times smaller than those for globular clusters accreted inside cored subhalos.

The above physical properties are lacking for most of the globular clusters with detected tidal tails. As far as we are aware, only M5 and NGC 288 have recently been targeted by A. E. Piatti (2023) and C. J. Grillmair (2025), respectively, from the selection of highest ranked tidal tail member candidates. A. E. Piatti (2023) found from the measurement of the dispersion of the tangential velocity that M 5 was accreted from a cuspy $\sim 10^9 M_\odot$ dark matter subhalo, in very good agreement with the overall consensus of being associated to the Helmi stream (T. M. Callingham et al. 2022, and reference therein). Similarly, C. J. Grillmair (2025) obtained a tangential velocity dispersion of stream candidates mostly consistent with having been stripped in a parent galaxy that had a large, cored dark matter halo. Indeed, NGC 288 is believed to have been brought into the Galactic halo during the Gaia-Enceladus-Sausage accretion event (V. Belokurov et al. 2018;

A. Helmi et al. 2018). In this context, S. M. Grondin et al. (2024) catalog opens the possibility to explore whether their mock extra-tidal stars are representative of tidal tails of globular clusters formed in situ. In Section 2, we describe the data handling and analysis, while in Section 3, we discuss the results. Section 4 summarizes the main conclusions of this work.

2. Data Analysis

The globular cluster extra-tidal star catalog generated by S. M. Grondin et al. (2024) contains 50,000 mock stars per globular cluster for a total of 159 globular clusters included in H. Baumgardt & M. Hilker (2018). The stars were simulated with the three-body particle spray code `Corespray` (S. M. Grondin et al. 2023), with their orbits integrated in the MWPot2014 model available in `galpy` (J. Bovy 2015). From the catalog, we retrieved R.A. and decl., proper motions along these celestial coordinates (μ_α^*, μ_δ), line-of-sight velocity ($V_{\rm los}$), heliocentric distance (d), galactocentric distance (R_{GC}), 3D galactic coordinates (X, Y, Z), and 3D action components (L_z, J_R, J_z) for a sample of globular clusters with a general consensus of being born in the bulge or in the disk of the Milky Way (see in situ origin criteria in T. M. Callingham et al. 2022, and references therein). We constrained the globular cluster sample to those with mock tidal tails longer than 1 kpc in any galactic direction, in order to secure a robust statistical analysis. With the aim of selecting the most suitable globular clusters, we visually inspected their mock tidal tails in the (X, Y, Z) galactic coordinate space and discarded those with extra-tidal features extending up to 1 kpc from their respective globular clusters' centers. Table 1 lists the resulting globular cluster sample.

One advantage of S. M. Grondin et al. (2024) catalog is that it provides Galactic coordinates for each star, so that we can deal with true physical dimensions of the tidal tails instead of great circle projections, which do not perform satisfactorily for highly radial tidal tails. Because angular positions of tidal tail stars have mostly been available, the vast majority of observation-based tidal tail studies have traced their properties along these angular directions in the sky (e.g., (R.A., decl.), (l, b), or (ϕ_1, ϕ_2)). Sometimes, the mean heliocentric distances of the respective globular clusters have also been adopted for all tidal tail members (see, e.g., S. Ferrone et al. 2023; C. Mateu 2023, and references therein). However, we aim at computing the widths, the dispersion in the z-component of the angular momentum, and in the line-of-sight and tangential velocities of tidal tails along them, so physical distances along the tidal tail from the associated globular cluster results are more appropriate. Employing angular distances can result in larger values of the analyzed quantities because of projection effects. Figure 1 depicts the spatial distribution of the mock extra-tidal stars of NGC 6496 in the (X, Y) Galactic planes (physical spatial distribution) compared to that in the projected celestial (R.A., decl.) coordinate system. As can be seen, projection effects are clearly visible in the celestial plane.

With the aim of tracing the properties of interest along the directions of the tidal tails of a globular cluster, we first built a stellar density map in the (X, Y, Z) space, and superposed on it 10 3D density level contours. The tidal tails of each globular cluster contain 50,000 mock stars, so that the sole number of mock stars located in a region is not indicative of the real presence of them. Instead, density levels illustrate more properly, statistically speaking, the tidal tail characteristics. The highest density level is at the globular cluster position. We then centered the coordinate system on the globular cluster and performed two perpendicular rotations in order to have the tidal tails mainly oriented along one of the three perpendicular axes. First, we rotated the galactic (X, Y, Z) system around the Y axis to the (X', Y, ϕ_3) system, as follows:

$$X' = X\cos(\theta) + Z\sin(\theta)$$

$$Y = Y$$

$$\phi_3 = -X\sin(\theta) + Z\cos(\theta),$$

where θ is the rotating angle to have the tidal tail in the (X, Z) plane aligned along the X' direction. Then, we rotated the (X', Y, ϕ_3) system around the ϕ_3 axis to the (ϕ_1, ϕ_2, ϕ_3) system, as follows:

$$\phi_1 = X'\cos(\psi) - Y\sin(\psi)$$

$$\phi_2 = X'\sin(\psi) + Y\cos(\psi)$$

$$\phi_3 = \phi_3,$$

where ψ is the rotating angle to have the tidal tail in the (X', Y) plane aligned along the ϕ_1 direction. The appropriate rotation angles θ and ψ were obtained by visually inspecting the orientation of the stellar density contours in the rotated 3D coordinate system. We called the rotated framework (ϕ_1, ϕ_2, ϕ_3), where ϕ_1 is along the tidal tails, ϕ_2 is perpendicular to ϕ_1 and contained in the tidal tails plane, and ϕ_3 is perpendicular to ϕ_1 and ϕ_2. Figure 2 illustrates the tidal tails of NGC 6496 in the (ϕ_1, ϕ_2) plane, with the stellar density levels corresponding to the 50% and 10% of the highest density level superimposed with a small and a large contour line, respectively. These stars represent the main substructures of the tidal tails. We note that the tidal tails' stars located outside the large contour were not used to compute the width, the dispersion in the z-component of the angular momentum, and in the line-of-sight and tangential velocities of tidal tails.

The next step consisted of plotting the z-component of the angular momentum, and the line-of-sight and tangential velocities as a function of ϕ_1 for all the stars located inside the stellar density volume corresponding to the 10% and 50% of the highest density level. The tangential velocities were computed as $V_{\rm Tan} = k \times d \times \mu$, where $k = 4.7405\ {\rm km\ s^{-1}\ kpc^{-1}\ (mas/yr)^{-1}}$, and $\mu = \sqrt{\mu_\alpha^{*2} + \mu_\delta^2}$. Figure 3 illustrates the resulting spatial distributions of L_z, $V_{\rm los}$, and $V_{\rm Tan}$ along the tidal tails direction (ϕ_1) of NGC 6496 for the 10% and 50% samples, represented with gray and orange points, respectively. We then fitted the observed distributions with polynomials of up to fifth order (see black and red curves in Figure 3 for 10% and 50% samples, respectively), which represent the mean behavior of the regarded physical properties along the tails. Finally, we computed the residuals (mock individual value − mean fitted value for the respective ϕ_1) and the respective standard dispersion, namely, σ_{L_z}, $\sigma_{V_{\rm los}}$, and $\sigma_{V_{\rm Tan}}$, which are quantities proposed by K. Malhan et al. (2021) and K. Malhan et al. (2022) to disentangle the origin of Milky Way globular clusters as formed in dwarf galaxies with central cored or cuspy dark matter profiles or formed in situ. The fourth proposed property, the tidal tails width (w), was computed from the residuals of the spatial distribution of stars in the (ϕ_2, ϕ_3) plane. Table 1 lists the resulting values for the selected globular clusters with origins in the bulge or in the disk of the Milky Way.

Table 1
Length, Width, and Dispersion in L_z, V_{los}, and V_{Tan} of Tidal Tails of Globular Clusters Formed in the Bulge/Disk of the Milky Way

Cluster	Origin	…	…	10% Sample	…	...	…	…	50% Sample	…	…
		Length (kpc)	w (pc)	$\sigma_{L_{\tilde{z}}}$ (km s^{-1} kpc)	$\sigma_{V_{los}}$ (km s^{-1})	$\sigma_{V_{Tan}}$ (km s^{-1})	Length (kpc)	w (pc)	$\sigma_{L_{\tilde{z}}}$ (km s^{-1} kpc)	$\sigma_{V_{los}}$ (km s^{-1})	$\sigma_{V_{Tan}}$ (km s^{-1})
Liller 1	bulge	2.7	200	41.4	80.0	98.4	1.1	110	36.0	81.1	97.3
NGC 6093	bulge	9.8	690	73.8	81.8	73.8	1.5	260	55.0	54.3	41.4
NGC 6144	bulge	2.9	80	22.3	15.0	20.5	1.0	50	17.9	12.3	14.5
NGC 6171	bulge	2.0	150	35.3	23.5	18.1	0.9	70	31.3	14.6	13.9
NGC 6266	bulge	2.5	160	60.9	54.5	36.6	0.6	80	56.0	47.7	31.7
NGC 6293	bulge	2.0	90	22.7	18.1	16.1	0.8	20	12.0	10.6	10.6
NGC 6325	bulge	1.0	40	11.7	18.4	13.6	0.3	10	6.2	7.9	10.4
NGC 6342	bulge	1.8	60	12.9	15.0	15.9	0.4	20	7.2	8.9	8.8
NGC 6380	bulge	1.0	150	33.3	31.7	24.3	0.4	40	34.9	16.7	16.3
NGC 6388	bulge	3.1	270	132.1	64.6	40.3	0.9	110	142.9	52.2	33.1
NGC 6401	bulge	1.7	60	27.4	48.6	36.6	0.4	20	10.7	19.9	16.7
NGC 6440	bulge	1.3	110	28.9	39.2	53.1	0.6	60	26.7	27.2	43.1
NGC 6453	bulge	2.3	130	35.6	29.3	22.1	0.4	30	30.1	11.6	13.8
NGC 6517	bulge	1.5	150	62.7	39.2	41.9	0.9	100	62.8	34.7	37.6
NGC 6522	bulge	1.0	40	11.2	19.5	21.2	0.4	30	12.7	15.7	14.6
NGC 6535	bulge	1.8	130	44.0	14.8	20.5	0.4	40	26.3	7.5	9.9
NGC 6558	bulge	1.3	50	17.4	29.3	37.0	0.4	40	16.3	20.3	28.6
NGC 6626	bulge	5.2	680	70.4	112.7	59.2	0.9	140	69.3	31.5	29.3
NGC 6637	bulge	2.0	100	15.6	24.0	24.7	0.7	50	10.1	17.2	13.3
NGC 6652	bulge	5.8	270	30.5	64.9	33.6	1.3	100	22.4	36.8	14.8
NGC 6723	bulge	3.7	90	19.7	41.5	35.6	0.8	40	7.6	24.5	19.4
Pal 6	bulge	4.3	150	30.0	60.1	42.0	1.0	70	21.3	25.2	16.5
Ter 1	bulge	2.1	200	48.0	49.1	20.0	0.5	70	43.0	35.0	14.7
Ter 6	bulge	2.3	760	22.7	30.3	25.4	0.4	40	17.3	17.5	18.9
VVV-cl001	bulge	5.1	120	60.1	66.7	43.5	0.8	90	47.6	182.6	70.2
IC 1276	disk	13.2	240	70.0	21.5	22.7	1.5	70	54.0	12.8	11.8
Lyngå 7	disk	3.0	180	51.6	16.4	32.7	0.7	60	50.0	12.0	17.9
NGC 5927	disk	12.1	400	82.5	24.9	26.4	1.2	120	84.7	16.2	20.6
NGC 6218	disk	3.6	220	52.4	25.6	21.6	1.8	120	48.2	17.1	18.7
NGC 6352	disk	2.6	120	34.2	14.5	15.3	1.5	80	30.9	11.7	12.5
NGC 6362	disk	3.2	160	43.6	13.0	16.6	0.8	60	50.6	10.7	12.6
NGC 6366	disk	3.4	170	48.2	21.1	18.3	0.7	50	50.5	10.9	12.3
NGC 6441	disk	5.2	890	185.6	74.3	44.3	2.0	340	174.5	49.6	37.1
NGC 6496	disk	3.8	140	41.6	16.5	14.3	1.0	80	31.2	12.7	11.7
NGC 6838	disk	6.6	200	66.9	14.4	16.4	0.8	70	44.6	7.0	8.3
Pal 10	disk	27.2	830	155.0	35.5	24.8	4.2	300	144.6	18.4	17.0
Pal 11	disk	4.4	140	46.9	9.3	7.2	1.1	70	41.8	6.7	5.5

3. Discussion

As mentioned in Section 1, the detection of tidal tails of globular clusters has been constrained by observational data depth and sky spatial coverage. S. Zhang et al. (2022) compiled a stringent list of globular clusters with studies of their surrounding fields focused on the search for extra-tidal structures. They followed the classification proposed by A. E. Piatti & J. A. Carballo-Bello (2020) of globular clusters with tidal tails (*T*), or with extended envelopes (*E*), or with no detection of extra-tidal structures (*N*) to label NGC 6362 with a T. None of the other studied globular clusters in this work (see Table 1) were included in their compilation. According to S. M. Grondin et al. (2024), the studied globular clusters have extra-tidal stars generated by three-body encounters in the clusters' cores that are distributed similarly to tidal tail stars. They can be visualized from the available version of their mock extra-tidal star catalog, accessible online at https://zenodo.org/record/8436703 (S. M. Grondin et al. 2023). From their stellar density maps, we found that the stellar density varies along the tidal tails (along ϕ_1), in the sense that the farther the position from the globular cluster, the lower the stellar density. There is somehow a representative stellar density level—corresponding to ∼10% of the highest density level—from which lower values of the stellar density do not follow the coherent stellar stream structure.

If we considered the stellar density levels (contours) of the tidal tails, the 50% sample would include every star located inside the so-called half-mass contour. Therefore, this sample of tidal tail stars is representative of the core features of the stellar stream. Because the tidal tails extend far beyond the half-mass contour, we also used stars distributed throughout a larger extension of the tails to estimate their properties. In this respect, we found, by inspecting the studied globular cluster tidal tails, that the lowest stellar density level that still preserves a coherent large-scale tidal tails structure is that corresponding to the 10% of the highest density level. For lower stellar density levels, the stellar density maps of the tidal tails only present scattered low-density debris. Because spatially spread and very

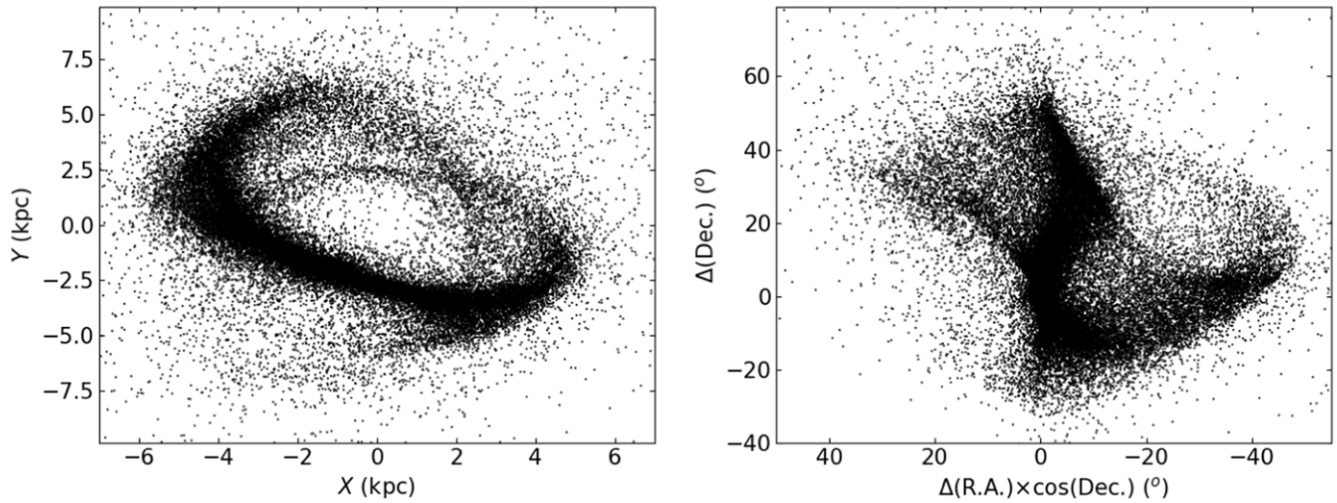

Figure 1. Distribution of tidal tail mock stars of NGC 6496 in the Galactic (X, Y) plane (left panel) and in the projected celestial (R.A., decl.) coordinate system (right panel).

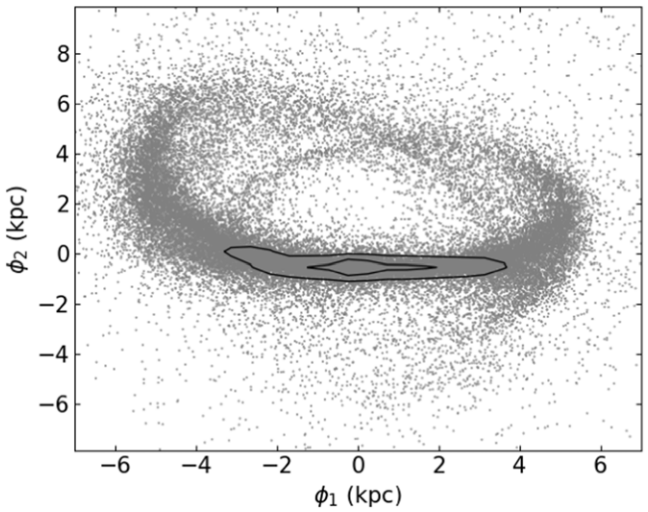

Figure 2. Same as the left panel of Figure 1 once the (X, Y, Z) coordinate system is rotated to the (ϕ_1, ϕ_2, ϕ_3) one. The smaller and larger contours correspond to the 50% and 10% of the highest stellar density level.

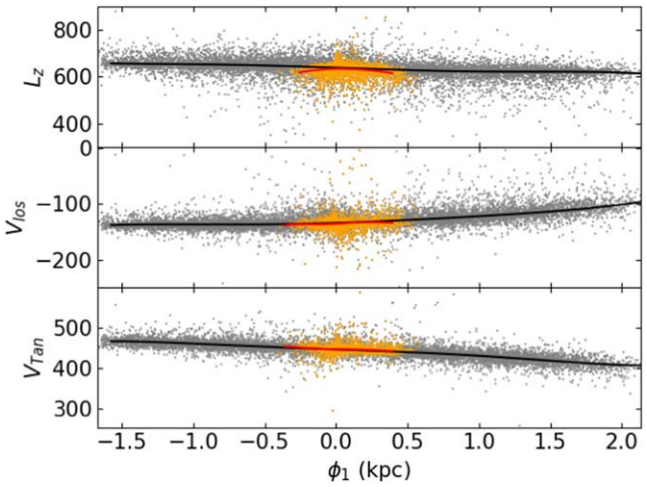

Figure 3. Variation of L_z, $V_{\rm los}$, and $V_{\rm Tan}$ along the tidal tails of NGC 6496, measured from the cluster's center. Gray and orange points represent stars contained within the stellar density contours corresponding to the 10% and 50% of the highest density level, respectively. Black and red solid lines represent the best-fitted polynomials to gray and orange points, respectively.

low stellar density substructures do not contribute to the main tidal tails features, we discarded them from our analysis.

Figure 4 shows the resulting distribution of w, σL_z, $\sigma V_{\rm los}$, and $\sigma V_{\rm Tan}$ values for the 10% and 50% samples, distinguished by dashed and solid histograms, respectively. Globular clusters formed in the bulge or in the disk of the Milky Way are colored red and blue, respectively. We then compared the widths and the dispersion in the z-component of the angular momentum, and in the line-of-sight and tangential velocities for the 10% and 50% samples. The ratio of the 10% sample to the 50% sample for these four properties resulted to be ∼1, which means that w, σL_z, $\sigma V_{\rm los}$, and $\sigma V_{\rm Tan}$ are on average constant along the considered extensions of the mock tidal tails. This means that in order to assess to what extent these mock tidal tails represent those real ones, we do not need to choose a stellar density level cut-off of the tidal tails to be used.

K. Malhan et al. (2021) found that the probability distribution functions of their simulations give values for the tidal tails width of $<$100 pc, and within ∼200–300, 300–400, 700–800, and 1600–2100 pc ($\pm 3\sigma$) for streams formed in situ, in cored dark matter profiles for masses of 10^8 and $10^9\,M_\odot$, and in cuspy dark matter profiles for masses of 10^8 and $10^9\,M_\odot$, respectively. The distribution of the resulting w values (see Figure 4) shows that only some streams are within the limits for an in situ formation. As far as the dispersion in the z-component of the angular momentum is considered, K. Malhan et al. (2021) predicted probability distributions with values $<$15 km s^{-1} kpc, and within ∼30–40, 50–90, 100–130, and 250–320 km s^{-1} kpc ($\pm 3\sigma$), respectively, for tidal tails of globular clusters formed in situ, in dwarf galaxies with 10^8 and $10^9\,M_\odot$ cored profiles of dark matter and in galaxies with 10^8 and $10^9\,M_\odot$ cuspy profiles of dark matter. Our values (10% and 50% samples) for the studied globular clusters point on average to a $10^8\,M_\odot$ central cored profile for the dark matter halo of the progenitor dwarf galaxy, in disagreement with their generally accepted in situ origin (T. M. Callingham et al. 2022, and references therein).

The dispersion in the line-of-sight and tangential velocities derived in this work and those obtained by K. Malhan et al. (2021) and K. Malhan et al. (2022) bring to light some differences. They obtained probability distribution functions for $\sigma_{V_{\rm los}}$ and $\sigma_{V_{\rm Tan}}$ that nearly overlap; the former being slightly

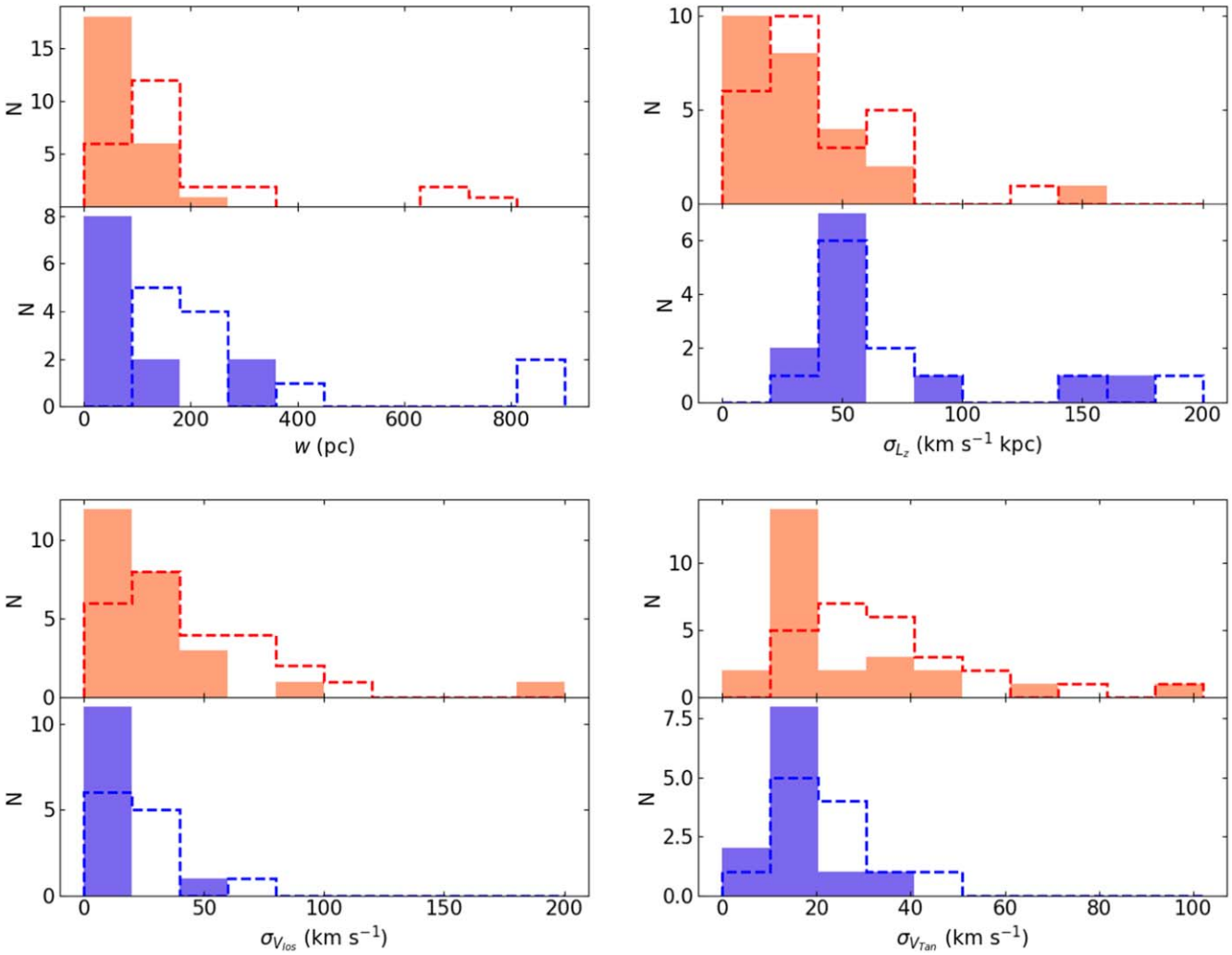

Figure 4. Distribution of the resulting w, σL_z, $\sigma V_{\rm los}$, and $\sigma V_{\rm Tan}$ values for the 10% and 50% samples, distinguished by dashed and solid histograms, respectively. Globular clusters formed in the bulge or in the disk of the Milky Way are colored red and blue, respectively.

larger. For streams formed in situ, they found values <1 km s^{-1}; for 10^8 and $10^9\,M_\odot$ cored dark matter profiles ($\pm3\sigma$) ~1–2 and <5 km s^{-1}; and for 10^8 and $10^9\,M_\odot$ cuspy dark matter profiles ($\pm3\sigma$) ~7–12 km s^{-1}. As can be seen, our values are, in general, inconsistent with any of the above values and, therefore, are in disagreement with the values for globular clusters formed in situ.

The larger values of velocity dispersion derived from the mock extra-tidal stars of S. M. Grondin et al. (2024) call our attention in light of recent line-of-sight velocity dispersion obtained from observational data and numerical simulations. For instance, M. Valluri et al. (2025) recently confirmed $\sigma_{V_{\rm los}} < 6$ km s^{-1} for the GD-1 stream, while R. Errani et al. (2022) found $\sigma_{V_{\rm los}} \sim 6$ km s^{-1} for the C-19 stream. A. E. Piatti (2023) obtained $\sigma_{V_{\rm Tan}} = 15.65 \pm 0.47$ km s^{-1} for M5, also favoring relatively high values for an accreted origin. However, these results do not reconcile the larger ones for the studied globular clusters (Table 1; 10% and 50% samples). Moreover, from orbit-averaged Monte Carlo globular cluster simulations and Milky Way–like cold dark matter cosmology simulations, N. C. Weatherford et al. (2024) and R. G. Carlberg & H. Agler (2023) found line-of-sight velocity dispersion of ~3–5 and <5 km s^{-1}, respectively, for tidal tails of globular clusters.

We investigated whether there exists any correlation between the widths and the dispersion in the z-component of the angular momentum, and in the line-of-sight and tangential velocities with the extension of the tidal tails. In order to do that, we considered the 50% sample, although overall behaviors for the 10% sample are in very good agreement with the former ones. Figure 5 depicts these correlations. First, globular clusters formed in the bulge or in the disk of the Milky Way have their tidal tails extension range overlapped; those formed in the bulge also have smaller tidal tails. We measured the extension of the stellar streams by computing the distance between the farthest stars located on both sides of the globular cluster's center. Second, both bulge and disk globular clusters show similar trends of the analyzed properties as a function of the stream length. Particularly, the width of the tidal tails increases with the stream length, a trend that would also seem to be the case for the dispersion of the z-component of the angular momentum. On the other hand, the dispersion in the line-of-sight and tangential velocities would not seem to increase with the stream length. As can be seen, there is an overall scatter around $\sigma V_{\rm los} \sim \sigma V_{\rm Tan} \sim 12$ km s^{-1} for any stream length, although much larger values are also obtained for globular clusters formed in the bulge of the Milky Way.

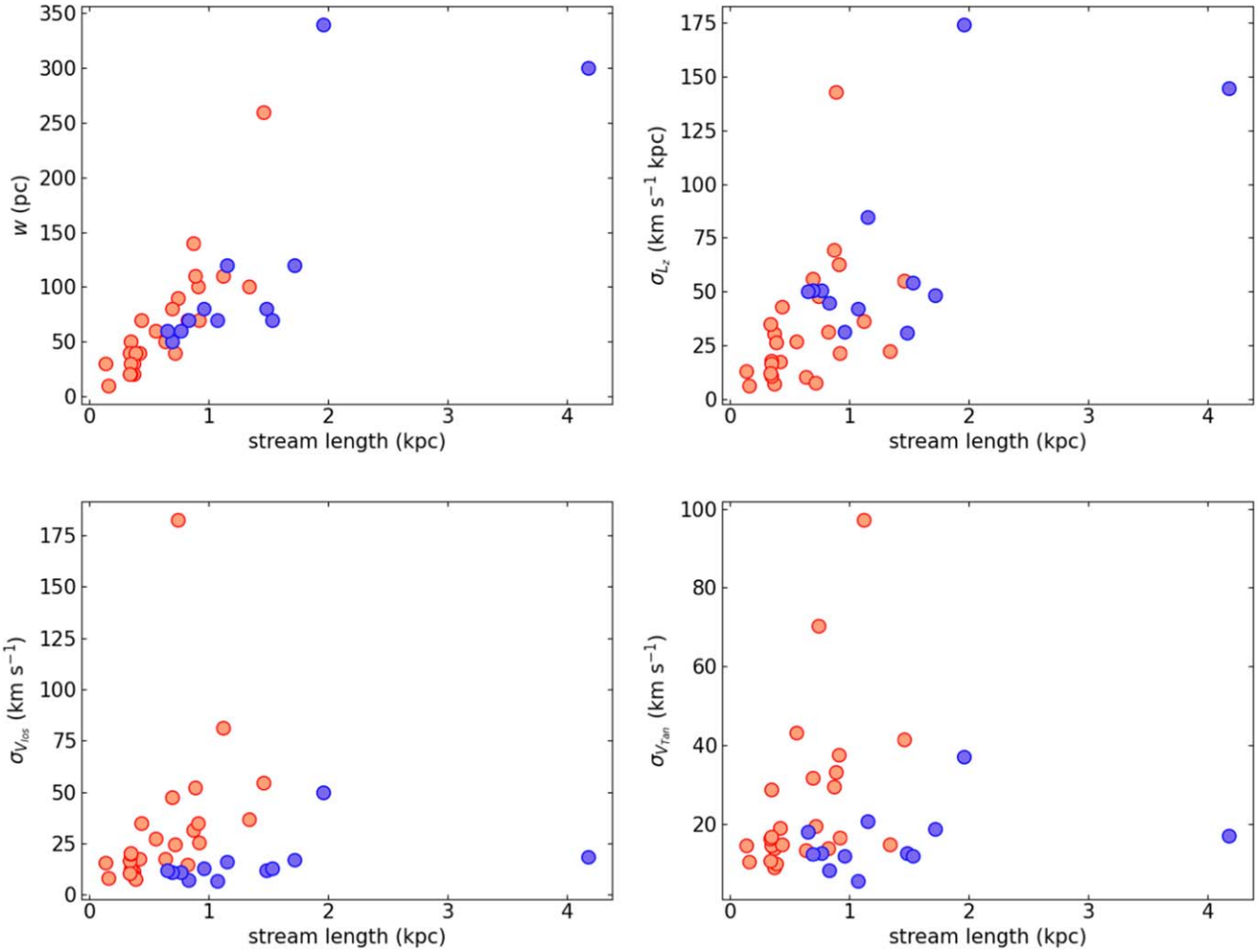

Figure 5. Relationship of w, σL_z, $\sigma V_{\rm los}$, and $\sigma V_{\rm Tan}$ values for the 50% sample with the stream length, measured as the distance between the farthest stars on both sides from the globular cluster's center. Globular clusters formed in the bulge or in the disk of the Milky Way are colored red and blue, respectively.

4. Conclusions

The tidal tails of globular clusters contain imprints of their formation and dynamical evolution. Despite their impact on our understanding of the formation of the Milky Way, it is still lacking globular clusters with bona fide tidal tail stars to estimate their physical properties. Recently, S. M. Grondin et al. (2024) generated a catalog of mock extra-tidal stars of Milky Way globular clusters, so we took advantage of them to assess at what extent they reproduce the values of physical properties of tidal tails, such as the tidal tail width, and the dispersion of the z-component of the angular momentum, and of the line-of-sight and tangential velocities (K. Malhan et al. 2021, 2022). Since S. M. Grondin et al. (2024) assumed their globular clusters' ejecta evolved fully in situ, we focused on globular clusters formed in the Milky Way.

In order to perform such an analysis, we selected a sample of globular clusters from the 159 included in the catalog, for which there exists an overall consensus of being formed in the bulge or in the disk of the Milky Way. This resulted in a self-consistent globular cluster sample suitable to carry out the aforementioned probe. We devised two different mock extra-tidal star samples for each globular cluster, aiming to represent the properties of the tidal tails out to the half-mass density contour (50% sample) and out to the outermost coherent substructure (10% sample), respectively. The former tells us about the characteristics of the tidal tail regions closer to its accompanying globular cluster, while the latter provides an overall picture of the tidal tails. After tracing the ridge line along the physical trailing–leading tails direction, we computed the four properties mentioned above following the recipes outlined in K. Malhan et al. (2021) and K. Malhan et al. (2022) to conclude that:

1. The width of the mock tidal tails, as well as the dispersion in L_z, $V_{\rm los}$, and $V_{\rm Tan}$ for both the 50% and 10% samples, resulted in them being similar to each other, respectively.
2. The values of the width of the tidal tails of only some studied globular clusters are in agreement with the expected range of values for an in situ origin in K. Malhan et al.'s (2021, 2022) models. The dispersion of the z-component of the angular momentum point to on average a $10^8\,M_\odot$ central cored profile dark matter halo of the progenitor dwarf galaxy, while the dispersion of the line-of-sight and of the tangential velocities are typically so large as to be inconsistent with any of the models from K. Malhan et al. (2021) and K. Malhan et al. (2022), in situ or otherwise. Therefore, the mock tidal tails of S. M. Grondin et al. (2024) of globular clusters formed

in situ would not seem to be similar to those of K. Malhan et al. (2021, 2022), nor to those studied in some observed globular clusters. This point may be worth making to the reader, especially as the framing of S. M. Grondin et al. (2024) and K. Malhan et al.'s (2021, 2022) works do not make this distinction immediately obvious.

3. The resulting L_z dispersion values and those for $V_{\rm los}$ and $V_{\rm Tan}$ point to either the consideration of other alternative formation scenarios for tidal tails associated with globular clusters formed in situ to be explored, or a more constrained sample of mock extra-tidal stars should be used in order to match the reference values. The present work does highlight a seeming modeling discrepancy that, while not necessarily a problem (due to large differences in the model construction designed to capture different regimes of globular cluster ejecta), is still worth clarifying to avoid confusion in further studies and avoid application of the relevant models in regimes they were not intended for.
4. Globular clusters formed in the bulge or in the disk of the Milky Way span similar stream length ranges, and their w, σL_z, $\sigma V_{\rm los}$, and $\sigma V_{\rm Tan}$ values also show similar correlations as a function of the stream length. The widths and the dispersion in L_z increase with the stream length, while the bulk of dispersion values in $V_{\rm los}$ and $V_{\rm Tan}$ are $\sim$12 km s^{-1} along the mock streams.

Acknowledgments

We thank the referee for the thorough reading of the manuscript and timely suggestions to improve it.

Data used in this work are available upon request to the author.

ORCID iDs

Andrés E. Piatti https://orcid.org/0000-0002-8679-0589

References

Baumgardt, H., & Hilker, M. 2018, MNRAS, 478, 1520
Belokurov, V., Erkal, D., Evans, N. W., Koposov, S. E., & Deason, A. J. 2018, MNRAS, 478, 611
Binney, J., & Tremaine, S. 2008, Galactic Dynamics: Second Edition
Bonaca, A., Pearson, S., Price-Whelan, A. M., et al. 2020, ApJ, 889, 70
Bovy, J. 2015, ApJS, 216, 29
Callingham, T. M., Cautun, M., Deason, A. J., et al. 2022, MNRAS, 513, 4107
Carlberg, R. G., & Agler, H. 2023, ApJ, 953, 99
de Boer, T. J. L., Erkal, D., & Gieles, M. 2020, MNRAS, 494, 5315
Errani, R., Navarro, J. F., Ibata, R., et al. 2022, MNRAS, 514, 3532
Ferrone, S., Di Matteo, P., Mastrobuono-Battisti, A., et al. 2023, A&A, 673, A44
Grillmair, C. J. 2022, ApJ, 929, 89
Grillmair, C. J. 2025, ApJ, 979, 75
Grondin, S. M., Webb, J. J., Lane, J. M., Speagle, J. S., & Leigh, N. W. 2023, A Catalogue of Galactic GEMS: Globular Cluster Extra-tidal Mock Stars, Zenodo, doi:10.5281/zenodo.8436703
Grondin, S. M., Webb, J. J., Lane, J. M. M., Speagle, J. S., & Leigh, N. W. C. 2024, MNRAS, 528, 5189
Grondin, S. M., Webb, J. J., Leigh, N. W. C., Speagle, J. S., & Khalifeh, R. J. 2023, MNRAS, 518, 4249
Helmi, A., Babusiaux, C., Koppelman, H. H., et al. 2018, Natur, 563, 85
Malhan, K., Ibata, R. A., Carlberg, R. G., et al. 2019, ApJL, 886, L7
Malhan, K., Valluri, M., & Freese, K. 2021, MNRAS, 501, 179
Malhan, K., Valluri, M., Freese, K., & Ibata, R. A. 2022, ApJL, 941, L38
Mateu, C. 2023, MNRAS, 520, 5225
Piatti, A. E. 2023, MNRAS, 525, L72
Piatti, A. E., & Carballo-Bello, J. A. 2020, A&A, 637, L2
Spitzer, L., & Shapiro, S. L. 1972, ApJ, 173, 529
Valluri, M., Fagrelius, P., Koposov, S. E., et al. 2025, ApJ, 980, 71
Weatherford, N. C., Kıroğlu, F., Fragione, G., et al. 2023, ApJ, 946, 104
Weatherford, N. C., Rasio, F. A., Chatterjee, S., et al. 2024, ApJ, 967, 42
Zhang, S., Mackey, D., & Da Costa, G. S. 2022, MNRAS, 513, 3136